Nonhazardous Solvent Systems for Processing Perovskite Photovoltaics

Kira L. Gardner, Jeffrey G. Tait, Tamara Merckx, Weiming Qiu, Ulrich W. Paetzold, Lucinda Kootstra, Manoj Jaysankar, Robert Gehlhaar, David Cheyns, Paul Heremans, and Jef Poortmans*

Replacing toxic solvents with nonhazardous solvents is one of the key challenges for industrial scale commercialization of thin film perovskite photovoltaics. Here, nonhazardous solvent/alcohol/acid systems are presented for the single-step deposition of pinhole-free perovskite layers with combined lead halide precursors of $Pb(CH_3CO_2)_2{\cdot}3H_2O$, $PbCl_2$, and CH_3NH_3I. Comparable performance to standard hazardous inks is achieved: devices with 15.1% power conversion efficiency are demonstrated and maintain 13.5% tracked for 5 min at maximum power point. Blade coated 4 cm^2 solar modules fabricated with highest performing device ink attain 11.9% in power conversion efficiency.

1. Introduction

Hybrid organometallic halide perovskites have rapidly become a front runner in the area of cost-effective semiconducting material for thin film photovoltaics, attaining certified 22.1% in power conversion efficiency for single junction solar cells.[1,2] Methylammonium lead halide perovskites, i.e., $CH_3NH_3PbI_3$, are solution processable, have a controllable direct band gap,[3] are tolerant to defects,[4,5] and combine a sharp absorption edge and high diffusion length with low absorption depth.[6] This combination of characteristics drive the field's progress. Mixed lead precursors, hydrated lead acetate ($PbAc_2$), and lead chloride ($PbCl_2$), can be combined to increase solution miscibility and film performance in processing.[7] Solution deposition from both two-step[8,9] and single-step[10] processes have attained up to 19.4% efficiency in planar architecture,[11] and present a viable option for large scale manufacturing in the commercial market.

To date, single-step deposition of the perovskite layer is one of the fastest and most cost-effective processes.[12,13] This process is accomplished by suspending precursor materials in an ink system that is used to coat the substrate quickly and uniformly. Next, the layer is dried and annealed to obtain a topologically and morphologically optimal film. The control of fabrication processes and parameters is indispensable in the formation of the crystalline structure of perovskite.[14] Two-step and multistep processes that use quenching solvents have been reported for the control of crystallization, and while they reach high efficiencies they can complicate both the process and scalability.[15–17]

The majority of solvent systems implemented in literature for deposition of organometallic halide perovskites are hazardous to handle. Most prominent and widely used solvents are toxic *N,N*-dimethylformamide (DMF),[9,18] DMF homologue dimethylacetamide (DMAC),[10,19] skin penetrating dimethyl sulfoxide (DMSO),[20,21] and carcinogenic *N*-methyl-2-pyrrolidone (NMP).[17,22,23] Nonhazardous solvents that can reach the same power conversion efficiencies as these have not been reported. Although cosolvent combinations of hazardous and nonhazardous solvents[15,16] can reduce hazardous content, it still does not present ideal safe alternatives for processing. Importantly, occupational safety must be taken into account for operators in manufacturing and scientists in the lab, who may come into direct contact with the ink or inhale solvent ink fumes during fabrication. Investigation of alternatives to present perovskite processing methods offer an invaluable opportunity to further safe and upscale-able photovoltaic manufacturing techniques.

K. L. Gardner, J. G. Tait, Dr. T. Merckx, W. Qiu, Dr. U. W. Paetzold, L. Kootstra, M. Jaysankar, Dr. R. Gehlhaar, Dr. D. Cheyns, Dr. P. Heremans, Dr. J. Poortmans
IMEC-Partner of Solliance
Kapeldreef 75, 3001 Leuven, Belgium
E-mail: tait@imec.be

K. L. Gardner
Department of Material Engineering
Stanford University
Stanford, CA 94305, USA

J. G. Tait, W. Qiu, M. Jaysankar, Dr. P. Heremans, Dr. J. Poortmans
Department of Electrical Engineering
KULeuven
3001 Leuven, Belgium

L. Kootstra
Department of Applied Physics
TUDelft
2628 Delft, The Netherlands

Dr. J. Poortmans
Department of Materials Engineering
Universiteit Hasselt
3500 Hasselt, Belgium

DOI: 10.1002/aenm.201600386

In this work, we develop nonhazardous solvent systems for single-step fabrication of high performance planar perovskite photovoltaics, based on blends of γ-butyrolactone, cyclic carbonates, alcohols, acids, and other protonated carbon chains. We first establish a clear definition of operator-safe inks, and employ the Hansen solubility parameter model to produce a guideline for potential ratio combinations of nonhazardous solvents for perovskite processing.[24] From this evaluation, promising candidates of solvent systems were selected and stepwise evaluated for their ability (i) to suspend the precursors, (ii) reliably coat a substrate, and (iii) transform to pinhole-free perovskite layers. With both spin coating and blade coating, we fabricate solar cells and solar modules that maintain high performance under maximum power point conditions.

2. Results and Discussion

2.1. Determination of Candidate Nonhazardous Ink Systems

The definition of a safe solvent is complex, but can be roughly broken into categories of environmentally-safe and operator-safe, where the latter is our concern in this manuscript. Thus, the criterion by which solvents are chosen is nontoxicity to humans in terms of possible exposure during manufacturing. Only solvents that are nonhazardous, i.e., noncarcinogenic, not significantly percutaneously absorbable (not skin penetrating), not reprotoxic, and not acutely harmful are considered for processing (**Figure 1**). Flammability can be considered a secondary risk to safety, because it can be overcome with conscientious solvent mixing. The solvents we investigate are not as benign as water, but represent a step toward true nonhazardousness and offer some respite from the solvents typically implemented in labs currently. Moreover, standard personal protective equipment that is found in most labs offer protection from the solvent systems we develop, unlike requirements for butyl gloves with solvents such as DMSO.

Nonhazardous solvents that were considered in this work are ethanol (EtOH), 1-propanol (PrOH), isopropyl alcohol (IPA), γ-butyrolactone (GBL), dimethylethanolamine (DMEA), propylene carbonate (PC), toluene, acetic acid (AcOH), xylene, ethylene glycol, and diethyl ether (Figure 1). While not as safe as water, all of these solvents sufficiently satisfy our requirements for operator safety. The most common of the alcohols, EtOH, exhibits noticeably adverse health effects only from chronic oral ingestion generally due to substance abuse.[25] A higher alcohol with a longer carbon chain, PrOH, is categorized as a slight irritant and has no known liver toxicity to humans.[26] In regards to chronic substance abuse, GBL is similar to EtOH.[27] AcOH is classified as an irritant at a volume percent <25 vol% and as industrial vinegar <20 vol%.[28] The other components listed above are not without limited toxicity, but are prevalent

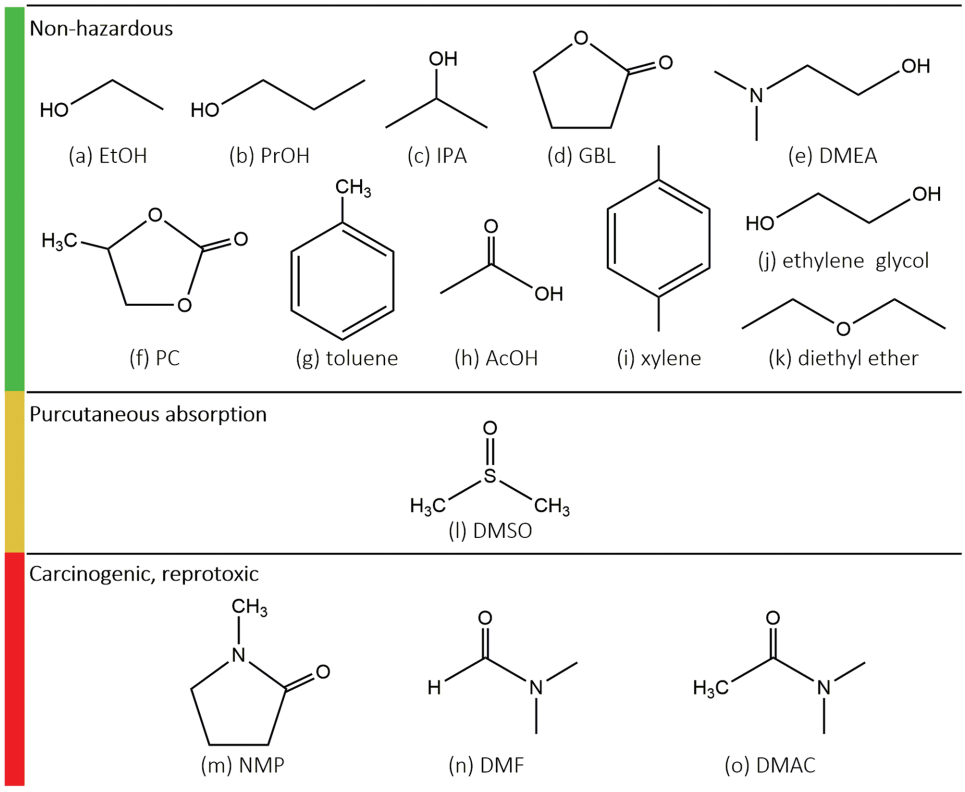

Figure 1. Diagram of increasing health concern for solvent options in precursor dissolution. Nonhazardous: a) ethanol, b) 1-propanol, c) isopropyl alcohol, d) γ-butyrolactone, e) DMEA, f) propylene carbonate, g) toluene, h) acetic acid, i) all forms of xylene (p-xylene is shown), j) ethylene glycol, and k) diethyl ether. Absorbable through skin: l) dimethyl sulfoxide. Carcinogenic and reprotoxic: m) *N*-methyl-2-pyrrolidone, n) *N*,*N*-dimethylformamide, and o) dimethylacetamide.

in industrial use, e.g. ethylene glycol is a common antifreeze, while xylene and toluene are typical paint thinners.

As a guideline, the Hansen solubility parameters (HSP) model can help to determine multi-solvent blends that are potentially miscible with perovskite precursors (CH_3NH_3I, $PbAc_2$, and $PbCl_2$), within the above nonhazardous requirements.[29] Hansen space can be defined in three intrinsic material variables: dispersion (δ_d), polarity (δ_p), and hydrogen bonding (δ_h). To find possible solvent combinations that are miscible with the precursors, the relative energy difference between the ink components and the precursors is minimized (Figure S1, Supporting Information). The HSP of toxic solvents like DMF, DMSO, and NMP provides a starting point for the solubility space of the precursors. We note that the solubility of the precursors in the proposed ink cannot be completely determined by HSP, because the simplicity of the model does not account for ionic interactions of salts nor molecular complexing. Using these parameters, the resulting minimized energy solvent combinations suggested by the model can be experimentally tested.

Analysis with HSP model of the nonhazardous solvents proposed above leads to the identification of promising combinations, including cyclic carbonates and active proton solvents like alcohols and acids.[29] Cyclic carbonates, alcohols, and acids provide a range of rheological parameters for deposition optimization. For cyclic carbonates, like GBL, greater solvent polarity enables higher salt miscibility, which can lead to denser film formation in a shorter drying time. However, these solvents typically have high viscosity and boiling points, which increases the evaporation stage of annealing. A high flash point is less sensitive to temperature fluctuations, and therefore safer, since there is low chance of spontaneous ignition. Protic solvents (such as EtOH and PrOH) that have a low flash point temperature can be paired with the higher boiling point cyclic carbonates to enhance safety, dissolve precursor salts, and take advantage of lower drying temperatures. Mitigating these undesirable qualities in individual solvents is possible with multiple components and can lead to safe and effective inks.

By implementing the HSP process described in the previous section, several possible solvent combinations are identified and tested with a range of volumetric ratios: GBL with PrOH, EtOH, IPA, AcOH, PC, and DMEA. The solubility for key ink ratios that were tested are listed in **Table 1**. Inks are considered soluble if the precursors dissolve with a concentration of at least 1 M, and nonsoluble if the ink displays precipitation for lower concentrations. Most promisingly, inks of GBL/alcohol/acid show solubility for inks containing at least 50 vol% GBL (**Figure 2**), below which these inks display colloidal separation. Inks with AcOH vol% > 20 vol% display a lower critical solution temperature characteristic, leading to decomplexing of the suspended salts and precipitation as the solution temperature increases.

Compiling all the solvents and systems investigated in this study enables the visualization of the HSP volume of solubility for the $PbAc_2/PbCl_2$/MAI precursor system (**Figure 3**). The visualized volume is not a regular ellipsoidal shape, which reduces the predicative capability of using relative energy difference as a guide rather than a law to miscible mixtures. A 3D visualization of the space is included in the Supporting Information (Figure S2). Moreover, the miscibility of an ink does not predict the film coatability nor the ability to convert to perovskite. These aspects have to be evaluated in subsequent steps.

Table 1. Solubility and ability to form perovskite in selected ink combinations.

Ink system	Volume [%]	>1 M Solubility	Perovskite formation
GBL	100	Y	Y
AcOH	100	N	N
EtOH	100	N	N
PrOH	100	N	N
PC	100	N	N
DMEA	100	Y	N
GBL/-/AcOH	60/-/40	Y	Y
GBL/EtOH/-	60/40/-	Y	Y
GBL/PrOH/-	60/40/-	Y	Y
GBL/PC/-	60/40/-	Y	N
GBL/DMEA/-	60/40/-	Y	N
GBL/EtOH/AcOH	60/20/20	Y	Y
GBL/PrOH/AcOH	60/20/20	Y	Y
GBL/PC/EtOH	60/20/20	Y	N
GBL/DMEA/EtOH	60/20/20	Y	N
DMF (hazard)	100	Y	Y
DMSO (hazard)	100	Y	Y
NMP (hazard)	100	Y	Y
DMAC (hazard)	100	Y	Y

2.2. Pinhole-Free Perovskite Layers

High efficiency perovskite solar cells require a dense and pinhole-free perovskite layer in order to ensure a high shunt resistance of the solar cell. Morphological pinholes in the perovskite absorber layer reduce device performance and photocarrier extraction by introducing shunt pathways and decreasing the effective active area.[14] Beyond the solvent system, processing parameters such as annealing conditions (time and temperature), rest time after initial layer application, and deposition technique can drastically affect film formation and must be controlled.[30]

All miscible solutions were spin coated and annealed to promote the formation of a perovskite thin film. Not all solvent systems that successfully dissolve precursor salts are able to form thin film perovskite layers (Table 1). Some of the promising nonhazardous solvents (DMEA and PC) do not convert to perovskite, which is likely due to stable complex formation.[15,31] Only solvent systems with GBL were further explored, as these films indicate the potential of successful perovskite formation. All inks that include GBL require 10 min longer compared to DMF-based inks to form the intermediate state after coating. Beyond the ability to convert to perovskite, layer morphology is important to control.

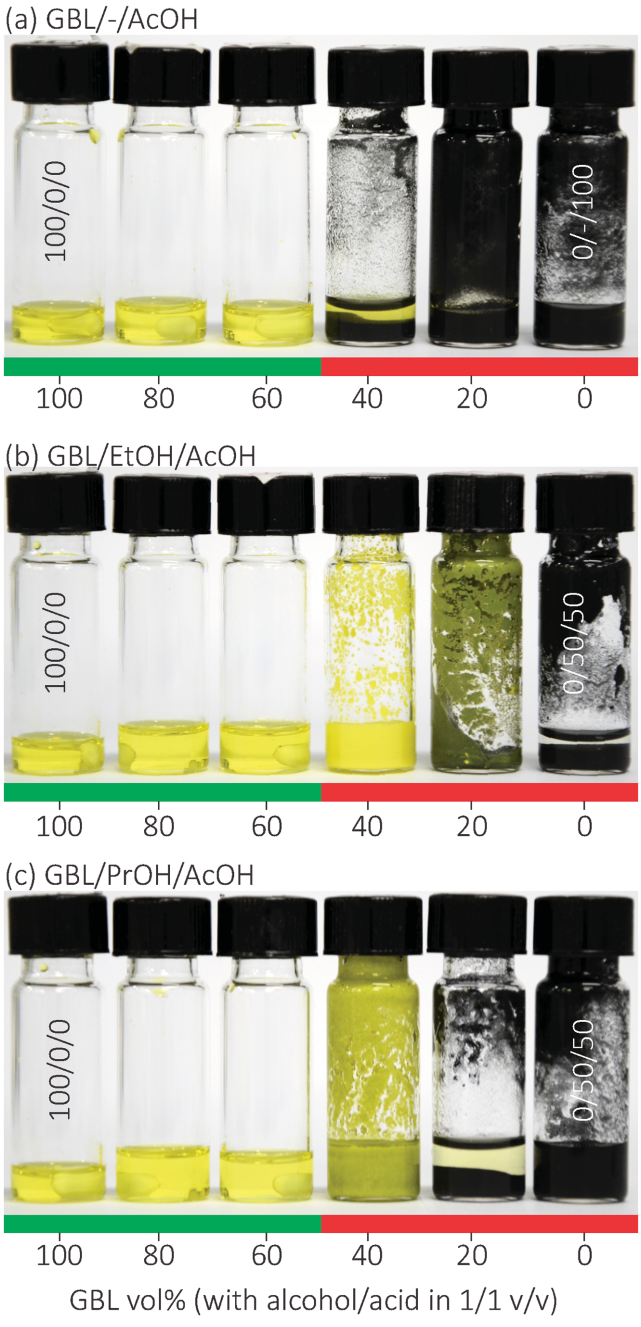

Figure 2. Photograph of inks based on decreasing vol% of GBL with equal parts alcohol/acid. All inks show precipitate formation for <50 vol% GBL for inks of a) GBL/-/AcOH, b) GBL/EtOH/AcOH, and c) GBL/PrOH/AcOH.

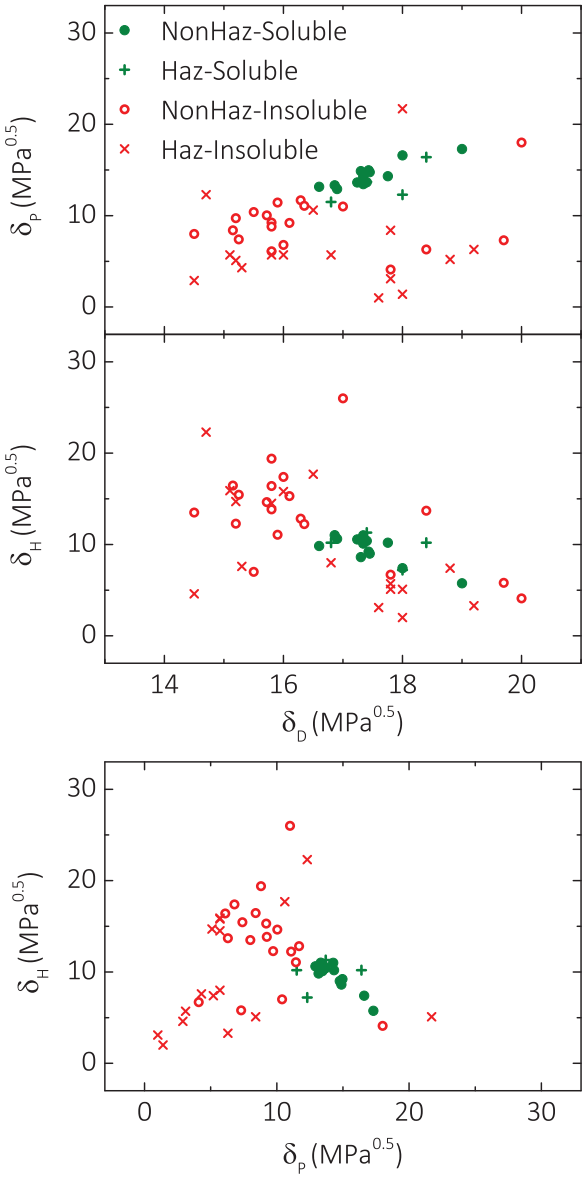

Figure 3. Hansen solubility parameter matrix plot of all investigated solvents and solvent systems for $PbAc_2/PbCl_2/MAI$ to at least 1 M PbX_2 and 3 M MAI. The parameters for inks that are hazardous (Haz) (circles) and nonhazardous (Nonhaz) (crosses) and that achieved either solubility (green) or were insoluble (red) are shown. A 3D representation of the parameter space helps to visualize the unique shape of the volume of solubility and is included in the Supporting Information.

The solutions that formed perovskite material were further screened for solvent ratios and coating conditions to attain pinhole-free perovskite layers after annealing at 140 °C for 10 min,[7] as described previously for this set of precursors. Solely GBL based inks form rough and pinhole riddled films of perovskite (**Figure 4**a). Increasing the combined alcohol/acid content from 0 to 40 vol% with GBL substantially increases surface coverage and reduces pinhole formation. Adding 20 vol% of AcOH, 10/10 vol% EtOH/AcOH or 10/10 vol% PrOH/AcOH to the solvent system reduces the pinhole size of the final perovskite layer while maintaining the same pinhole density (Figure 4c,d,e). Adding 40 vol% AcOH or 20/20 vol% PrOH/AcOH results in a lower pinhole density (Figure 4f,h). Pinhole-free layers can be achieved by adding 20/20 vol% EtOH/AcOH to GBL (Figure 4g), similar to those achieved with DMF-based inks (Figure 4b).

The addition of alcohol results in small-scale roughness in the middle of the grains (Figure 4e). The higher vapor pressure of the alcohol over the AcOH and GBL may cause this roughness, as "trapped" solvent near the substrate escapes

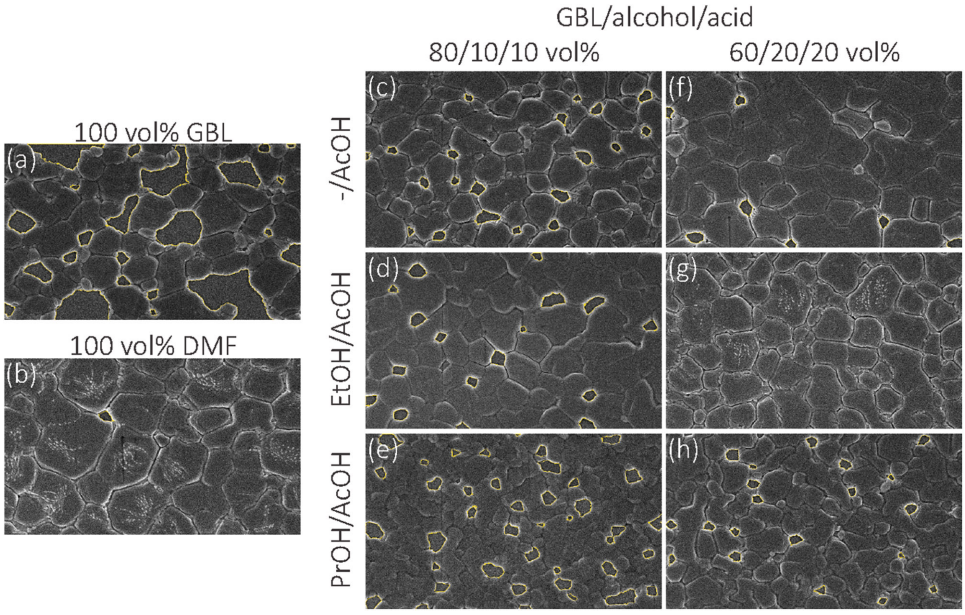

Figure 4. Top-view SEM images, with color outlined pinholes, of spin coated and annealed perovskite layers from the following solvent blends: a) GBL (100 vol%), b) DMF (100 vol%), c) GBL/-/AcOH (80/-/20 vol%), d) GBL/EtOH/AcOH (80/10/10 vol%), e) GBL/PrOH/AcOH (80/10/10 vol%), f) GBL/-/AcOH (60/-/40 vol%), g) GBL/EtOH/AcOH (60/20/20 vol%), and h) GBL/PrOH/AcOH (60/20/20 vol%).

through a top crust during the annealing process. Dissolution-recrystallization growth methods resulting in film formation have been shown to depend on both hydration and formation of intermediate complexes.[15,32] The polar and aprotic, and thus hydrophilic characteristics of DMF[31] are possibly being emulated in the fast evaporation of EtOH while AcOH assists in complexing to form the correct intermediate phase for perovskite formation.

Photospectroscopy and reflectivity X-ray diffraction (XRD) confirms the complete transformation to perovskite upon annealing for all the spin coated systems (**Figure 5**). The XRD peak indicative of the hexagonal lattice of PbI_2 ($2\theta = 12.55°$) in the film is negligible.[33] Diffraction peaks of the (110), (220), and (330) at 2θ of 14°, 28°, and 43°, respectively, are apparent in the XRD spectra. A bandgap of 1.55 eV is observed in the absorption onset for each solvent system involved. With high quality and pinhole-free perovskite layers now formed, photovoltaics devices can now be fabricated.

2.3. High Performance Spin Coated Perovskite Solar Cells

Photovoltaic devices with an n-i-p architecture[34] (ITO/TiO_2/perovskite/spiro-MeOTAD/Au) were fabricated for each perovskite-forming solution. The perovskite layers were spin coated in a single step onto a compact TiO_2 layer, as previously published (processing conditions in the Experimental Section).[35] The hole transporting material, spiro-MeOTAD was then spin coated prior to the evaporation of the Au contact.

The highest device performance was measured for GBL/EtOH/AcOH with *J–V*-measured power conversion efficiency of $\eta_{JV} = 15.1\%$ while the reference DMF-based device attained $\eta_{JV} = 16.7\%$ (**Figure 6**). The other solvent systems, with at least one acid or alcohol added, each attain $\eta_{JV} > 11\%$ (**Table 2**). The layer thickness was optimized for each ink by modifying the precursor concentration. We note that the V_{OC} of the devices from GBL based inks is consistently 60–80 mV lower than the DMF-based reference device, which we associate to non-optimal processing conditions. Variations in V_{OC} of perovskite devices have been extensively reported for different processing conditions. With further development, the deposition and annealing steps could be modified to reduce recombination[36] and increase the V_{OC} to at least the level of the reference device.

Regardless of the minimal observable hysteresis (Figure S3, Supporting Information) measured from the *J–V*, tracking the operation at the maximum power point under constant illumination and bias offers a more realistic view of the "initial" performance under operational conditions. Tracking the maximum power point for 5 min, the GBL/EtOH/AcOH devices and the reference DMF device decrease to the same efficiency of $\eta_{MPP} = 13.5\%$. The GBL/PrOH/AcOH devices also display a relative 15% drop in efficiency over the same period, decreasing to $\eta_{MPP} = 12\%$. Solvent systems without the combined alcohol/acid component each show large drops of >20% at the maximum power point. The process was tested for reproducibility and yield with 60 devices for each ink (Figure S4, Supporting Information), finding consistent results for devices independently fabricated under equal conditions.

2.4. Blade Coated Perovskite Solar Modules

The linear deposition technique of blade coating was used to probe the coating capability of the developed nonhazardous ink systems. Blade coating, a roll-to-roll compatible technique,

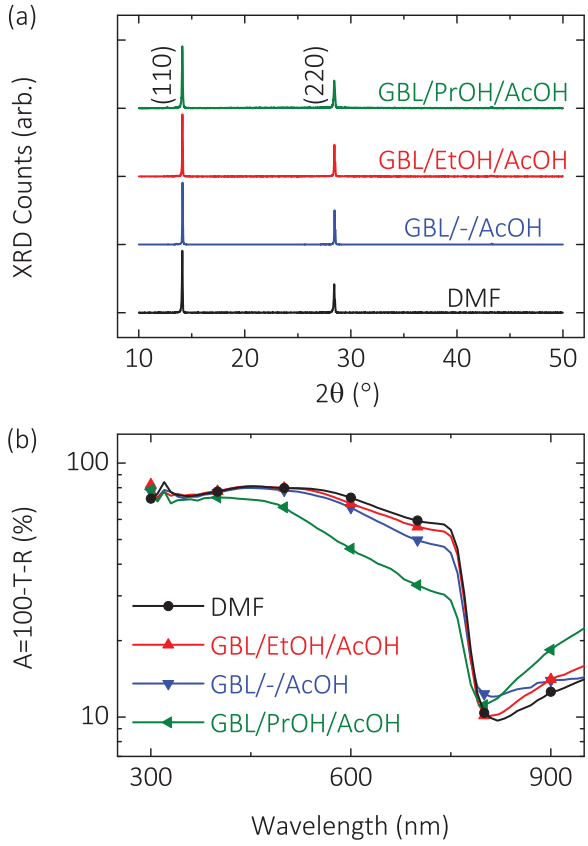

Figure 5. a) X-ray diffraction and b) absorptance spectra of perovskite films from the best performing solvent systems.

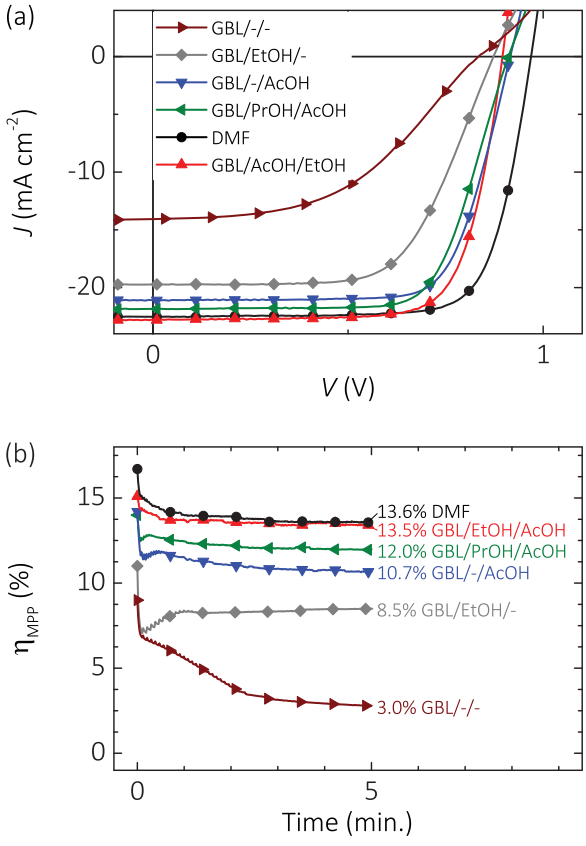

Figure 6. a) Current density versus voltage and b) maximum power point tracking under AM1.5G illumination of power conversion efficiency over 5 min for representative devices from each ink.

provides a high throughput with low material waste.[37] The highest density film coverage for blade coating was attained with the same ink as spin coating, GBL/EtOH/AcOH at 60/20/20 vol%. Under optimized coating conditions this ink forms smoother and more uniform films than standard DMF blade coating, potentially related to the reflow of the lower vapor pressure GBL ink.

Blade coated single solar cells from GBL/EtOH/AcOH (60/20/20 vol%) achieved *J*–*V* efficiency of η_{JV} = 14.5% and a maximum power point efficiency of η_{MPP} = 11.8% (Table 2, **Figure 7**). To demonstrate the high uniformity and scalability of linearly coating the perovskite layer from nonhazardous inks, we fabricated 4 cm^2 (aperture area) blade coated modules.[38] The process details for module preparation are described elsewhere.[7,35] The modules achieve an aperture area efficiency of η_{JV} = 11.9% and η_{MPP} = 8.2% (Figure 7), demonstrating the scalable potential of nonhazardous ink systems. The newly developed solvent system demonstrates not only the capability to suspend high concentrations of precursors, but also to be generally applicable to both spin and linear deposition techniques and to large area coating for thin film photovoltaic modules.

Table 2. Device and module performance metrics for nonhazardous solvent systems.

Solvent system	Volume [%]	V_{OC} [V]	J_{SC} [mA cm^{-2}]	FF [%]	η_{JV} [%]	η_{MPP} [%]
GBL/-/-	100/0/0	0.83	16.6	59	9.0	3.0
GBL/EtOH/-	60/40/0	0.88	18.8	62	11.0	8.5
GBL/-/AcOH	60/0/40	0.89	19.3	73	14.1	10.7
GBL/EtOH/AcOH	60/20/20	0.88	21.2	71	15.1	13.5
GBL/PrOH/AcOH	60/20/20	0.90	17.2	72	14.0	12.0
DMF	100	0.96	21.9	74	16.7	13.6
Cell-Blade$_{GBL/EtOH/AcOH}$	60/20/20	0.89	21.1	73	14.5	11.8
Module-Blade$_{GBL/EtOH/AcOH}$	60/20/20	3.35	5.1	69	11.9	8.2

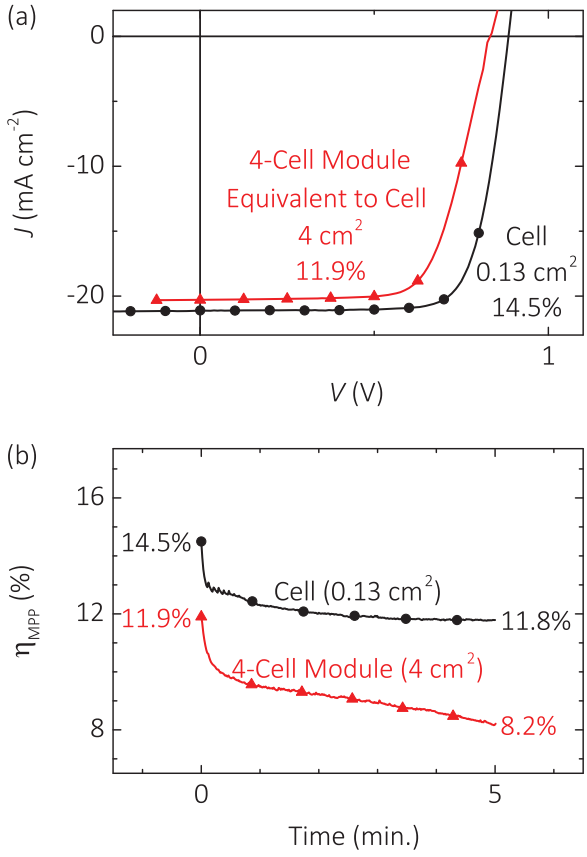

Figure 7. a) Equivalent current density versus voltage and b) maximum power point tracking under AM1.5G illumination of power conversion efficiency over 5 min for blade coated cells and modules from GBL/EtOH/AcOH. For visual comparison, the module *J–V* is the cell-equivalent measurement from a module.

3. Conclusions

In conclusion, we have developed a set of nonhazardous ink systems for single-step coating of methylammonium lead halide (with spectator ion) perovskite layers based on solvent, alcohol, and acid mixtures. With γ-butyrolactone/ethanol/acetic acid (60/20/20 vol%), performance of $\eta_{JV} = 15.1\%$ was achieved, and maintained $\eta_{MPP} = 13.5\%$ after 5 min of maximum power point tracking under constant illumination, results equivalent to reference dimethylformamide-based devices. The same ink was implemented with scalable blade coating to attain cell performance $\eta_{JV} = 14.5\%$ and $\eta_{MPP} = 11.8\%$, while 4 cm^2 modules performed with $\eta_{JV} = 11.9\%$ and $\eta_{MPP} = 8.2\%$. While the deposition of this ink system provided pinhole-free films, other combinations of solvent/alcohol/acid which show promise in device fabrication should be further optimized for scalable coating techniques. Moreover, this ink or a related solvent system, may continue to function with lead-free precursor systems, while the development process implemented here can be imitated with each new material set. This work drives single-step perovskite deposition processes another step toward industrial scale commercialization.

4. Experimental Section

Device Fabrication: Indium-doped transparent tin oxide coated glass was purchased from Colorado Concepts and cleaned using a 5 min ultrasonic bath in detergent, deionized water, acetone, and iso-propyl alcohol. A layer of 20 nm thick TiO_2 was then deposited via reactive electron beam evaporation in vacuum at an oxygen pressure of 2.0×10^{-4} Pa, as reported previously.[35] Solid $PbCl_2$ (Sigma-Aldrich), $Pb(CH_3CO_2)_2{\cdot}3H_2O$ (Sigma-Aldrich), and CH_3NH_3I (Dyesol) were mixed at a ratio of 0.2:0.8:3.0 M, respectively. This precursor powder was then dissolved in each ink system at room temperature and agitated for 1 h at room temperature. The Pb-precursor concentration in each of the solutions varied from 0.7 to 1.0 M depending on thickness optimization. Each solution was coated on the TiO_2-coated ITO glass substrate by spin-coating at 2000 rpm for 60 s, dried until visual formation of intermediate brown film was observed (approximately 10 min) and then annealed on a hot plate at 140 °C for 10 min. All steps from spin-coating on were carried out in an N_2 environment. Initial testing of solvent system film formation was performed with spin coating for its ease of testing, but can eventually be implemented with scalable techniques like blade coating when successful solvent systems are identified. Blade coating was carried out on a 40 °C hotplate at a blade speed of 100 mm s^{-1} and about 75% of the concentration used in spin coated layers. Next, the organic hole transporting layer (80 mg spiro-OMeTAD (2,2',7,7'-tertrakis(N,N-di-p-methoxyphenilamine)-9,9'-spirobifluorene) in 1 mL chlorobenzene), 28.5 µL 4-tert-butyl-pyridine, 17.5 µL of 520 mg lithium-bis (trifluoromethanesulfonyl) imide (Li-TFSI) in 1 mL of acetonitrile) was deposited via spin-coating at 1000 rpm for 60 s. Lastly, an 80 nm thick gold electrode was deposited by thermal evaporation in vacuum at a pressure of $<2.0 \times 10^{-6}$ Pa.

Device Characterization: The current–voltage (*I–V*) curves of the photovoltaic devices were measured in an N_2 glove box using a Keithley 2602A Source-Measure Unit and class A Abet solar simulator producing 100 mW cm^{-2} AM1.5G illumination. These curves were recorded between −1.2 and 0.5 V with 0.01 V steps and a delay of 0.01 s for a scan speed of 1 V s^{-1}. Initial light soaking was required for devices fabricated from non-DMF solvent systems and could be up to 10 min before a maximum steady efficiency was obtained. To overcome the error that hysteresis introduced to the measurement and to measure performance in a model closer to the real operating conditions, maximum power point tracking was implemented under continuous illumination. Maximum power point tracking using a perturb and observe method under continuous illumination. The bias was kept constant while the current was measured every 50 power line cycles. Crystallographic structure of the perovskite was determined with Bragg Brentano style XRD using a PANalytical X'Pert Pro Materials Research Diffractometer using the Cu Kα line at an incident angle of 0.2°. The scanning electron microscope images were taken with a FEI Nova 200 scanning electron microscope. The reflection/transmission was measured with coupled and monochromated Xe and quartz halogen lamps, and an integrating sphere calibrated with an Si photodiode.

Acknowledgements

K.L.G. and J.G.T. contributed equally to this work. The work of K.L.G. was supported by the Roger Van Overstraeten Society. The work of J.G.T. was partially supported by the Natural Science and Engineering Research Council of Canada. The work of U.W.P. was supported by the German Academic Exchange Service. This work has been partially supported by Solliance, a partnership of R&D organizations from Belgium, the Netherlands, and Germany working in thin film photovoltaic solar energy.

Received: February 22, 2016
Revised: March 23, 2016
Published online: May 27, 2016

[1] NREL Efficiency Chart, March **2016**.
[2] M. A. Green, K. Emery, Y. Hishikawa, W. Warta, E. D. Dunlop, *Prog. Photovolt.: Res. Appl.* **2016**, *24*, 3.
[3] W. Yin, J. Yang, J. Kang, Y. Yan, S.-H. Wei, *J. Mater. Chem. A* **2015**, *3*, 8926.
[4] D. Shi, V. Adinolfi, R. Comin, M. Yuan, E. Alarousu, A. Buin, Y. Chen, S. Hoogland, A. Rothenberger, K. Katsiev, Y. Losovyj, X. Zhang, P. A. Dowben, O. F. Mohammed, E. H. Sargent, O. M. Bakr, *Science* **2015**, *347*, 519.
[5] W. S. Yang, J. H. Noh, N. J. Jeon, Y. C. Kim, S. Ryu, J. Seo, S. I. Seok, *Science* **2015**, *348*, 1234.
[6] G. Xing, N. Mathews, S. Sun, S. S. Lim, Y. M. Lam, M. Gratzel, S. Mhaisalkar, T. C. Sum, *Science* **2013**, *342*, 344.
[7] W. Qiu, T. Merckx, M. Jaysankar, C. Masse de la Huerta, L. Rakocevic, W. Zhang, U. W. Paetzold, R. Gehlhaar, L. Froyen, J. Poortmans, D. Cheyns, H. J. Snaith, P. Heremans, *Energy Environ. Sci.* **2016**, *9*, 484.
[8] J. Burschka, N. Pellet, S.-J. Moon, R. Humphry-Baker, P. Gao, Md. K. Nazeeruddin, M. Gratzel, *Nature* **2013**, *499*, 316.
[9] C.-G. Wu, C.-H. Chiang, Z.-L. Tseng, Md. K. Nazeeruddin, A. Hagfeldt, M. Gratzel, *Energy Environ. Sci.* **2015**, *8*, 2725.
[10] D. Shen, X. Yu, X. Cai, M. Peng, Y. Ma, X. Su, L. Xiao, D. Zou, *J. Mater. Chem. A* **2014**, *2*, 20454.
[11] Y. Shao, Y. Yuan, J. Huang, *Nat. Energy* **2016**, *1*, 15001.
[12] I. Burgués-Ceballos, M. Stella, P. Lacharmoise, E. Martínez-Ferrero, *J. Mater. Chem. A* **2014**, *2*, 17711.
[13] Y. Deng, E. Peng, Y. Shao, Z. Xiao, Q. Dong, J. Huang, *Energy Environ. Sci.* **2015**, *8*, 1544.
[14] D. T. Moore, H. Sai, K. W. Tan, D.-M. Smilgies, W. Zhang, H. J. Snaith, U. Wiesner, L. A. Estroff, *J. Am. Chem. Soc.* **2015**, *137*, 2350.
[15] N. Ahn, D.-Y. Son, I.-H. Jang, S. M. Kang, M. Choi, N.-G. Park, *J. Am. Chem. Soc.* **2015**, *137*, 8696.
[16] N. J. Jeon, J. H. Noh, Y. C. Kim, W. S. Yang, S. Ryu, S. I. Seok, *Nat. Mater.* **2014**, *13*, 897.
[17] Y. Zhou, M. Yang, W. Wu, A. L. Vasiliev, K. Zhu, N. P. Padture, *J. Mater. Chem. A* **2015**, *3*, 8178.
[18] T. H. Kim, S. G. Kim, *Saf. Health Work* **2011**, *2*, 97.
[19] M. Lv, X. Dong, X. Fang, B. Lin, S. Zhang, J. Ding, N. Yuan, *RSC Adv.* **2015**, *5*, 20521.
[20] J. Galvao, B. Davis, M. Tilley, E. Normando, M. R. Duchen, M. F. Cordeiro, *FASEB J.* **2014**, *28*, 1317.
[21] J. H. Noh, S. I. Seok, *MRS Bull.* **2015**, *40*, 648.
[22] W. Nie, H. Tsai, R. Asadpour, J.-C. Blancon, A. J. Neukirch, G. Gupta, J. J. Crochet, M. Chhowalla, S. Tretiak, M. A. Alam, H.-L. Wang, A. D. Mohite, *Science* **2015**, *347*, 522.
[23] L. A. Malley, G. L. Kennedy, G. S. Elliot, T. W. Slone, W. Mellert, K. Deckardt, K. Kuttler, B. Hildebrand, M. I. Banton, R. J. Parod, J. C. Griffiths, *Drug Chem. Toxicol.* **2001**, *24*, 315.
[24] J. G. Tait, T. Merckx, W. Li, C. Wong, R. Gehlhaar, D. Cheyns, M. Turbiez, P. Heremans, *Adv. Funct. Mater.* **2015**, *25*, 3393.
[25] F. Yang, J. Luo, *Biomolecules* **2015**, *5*, 2538.
[26] S. Laham, M. Potvin, K. Schrader, I. Marino, *Drug Chem. Toxicol.* **1980**, *3*, 343.
[27] L. J. Schep, K. Kundsen, R. J. Slaughter, J. A. Vale, B. Megarbane, *Clin. Toxicol.* **2012**, *50*, 458.
[28] *Toxicity Profile: Acetic acid and Its Common Salts* **1993**, BIBRA Toxicology Advice and Consulting, Wallington, Surrey, UK.
[29] C. M. Hansen, *Hansen Solubility Parameters: A User's Handbook,* CRC Press, Inc., Boca Raton, FL **1999**, pp. 70–95.
[30] G. E. Eperon, V. M. Burlakov, P. Docampo, A. Goriely, H. J. Snaith, *Adv. Funct. Mater.* **2014**, *24*, 151.
[31] K. Yan, M. Long, T. Zhang, Z. Wei, H. Chen, S. Yang, J. Xu, *J. Am. Chem. Soc.* **2015**, *137*, 4460.
[32] Y. Fu, F. Meng, M. B. Rowley, B. J. Thompson, M. J. Shearer, D. Ma, R. J. Hamers, J. C. Wright, S. Jin, *J. Am. Chem. Soc.* **2015**, *137*, 5810.
[33] A. Alberti, I. Deretzis, G. Pellegrino, C. Bongiorno, E. Smecca, G. Mannino, F. Giannazzo, G. G. Condorelli, N. Sakai, T. Miyasaka, C. Spinella, A. La Magna, *ChemPhysChem* **2015**, *16*, 3064.
[34] H. J. Snaith, *J. Phys. Chem. Lett* **2013**, *4*, 3623.
[35] W. Qiu, U. W. Paetzold, R. Gehlhaar, V. Smirnov, H.-G. Boyen, J. G. Tait, B. Conings, W. Zhang, C. B. Nielsen, I. McCulloch, L. Froyen, P. Heremans, D. Cheyns, *J. Mater. Chem. A* **2015**, *3*, 22824.
[36] Q. Chen, H. Zhou, T.-B. Song, S. Luo, Z. Hong, H.-S. Duan, L. Dou, Y. Liu, Y. Yang, *Nano Lett.* **2014**, *14*, 4158.
[37] Y. Chang, S. Tseng, C. Chen, H. Meng, E. Chen, S. Horng, C. Hsu, *Org. Electron.* **2009**, *10*, 741.
[38] J. G. Tait, S. Manghooli, W. Qiu, L. Rakocevic, L. Kootstra, M. Jaysankar, C. Masse de la Huerta, U. W. Paetzold, R. Gehlhaar, D. Cheyns, P. Heremans, *J. Mater. Chem. A* **2016**, *4*, 3792.